*Proceedings of the Twenty-Sixth Asilomar Conference on Signals, Systems & Computers,*
Pacific Grove, CA, October 26–28, 1992

# Performance Evaluation of Cyclic Polyspectrum Estimators*

Chad M. Spooner William A. Gardner
Department of Electrical and Computer Engineering
University of California
Davis, CA 95616

## Abstract

*Results of analysis and computer simulations are used to compare two methods of estimating the cyclic polyspectrum. The computational requirements of the two methods are determined and compared. A cycle leakage phenomenon is explained and it is shown that, for a given amount of data, only one of the two methods can be modified to reduce this leakage, but at the cost of increased computations. Numerical examples of measurements of fourth-order cyclic polyspectra are provided to illustrate the leakage problem.*

## 1 Introduction

There has been a large effort in recent years to develop the theory of higher-order statistics of stationary random processes and to apply it to certain signal processing problems. There has also been a smaller, but persistent, effort during the last twenty years to develop and apply the theory of second-order cyclostationary (CS) time-series. Elements of both theories can be found in the study of the higher-order statistics of CS signals, which shows potential for use in signal detection and parameter estimation. To realize this potential, however, the large computational cost of estimating the parameters of the theory must be minimized, and the statistical behavior of these estimators must be understood.

In this paper, two methods of computing estimates of the cyclic polyspectrum (CP) are evaluated and compared in terms of accuracy and computational cost. The CP is the generalization of the polyspectrum [1, 6] from stationary to CS signals, and is the generalization of the cyclic spectrum [2] to higher orders. The CP is the central frequency-domain parameter in the study of higher-order cyclostationarity (HOCS), which is the study of higher-order temporal and spectral moments and cumulants of CS signals [8, 10]. The CP can be estimated by using a time-domain method, in which the $n$th-order cyclic temporal cumulant is estimated, windowed, and Fourier transformed, or by using a frequency-domain method, in which the $n$th-order cyclic periodogram is multiplied by a special masking function, and then convolved with a multidimensional window function. The former can be thought of as a generalization of the Blackman-Tukey method of spectrum estimation to higher-orders, whereas the latter can be thought of as a generalization of the Wiener-Daniell method [2]. The generalization of the Bartlett-Welch method of spectrum estimation — time-averaging the $n$th-order cyclic periodogram — is not considered because of limited space (see [7, 8]).

The analysis framework used herein is the nonstochastic time-average framework, which is explained in detail in [2] and in relation to HOCS in [7, 8, 9]. This framework obviates the concept of (cyclo)ergodicity, and thereby avoids certain mathematical difficulties associated with the estimation of the CP ([8], Chapter 6).

The reader may wonder why the subject of HOCS is of interest at all, much less the details of measuring its parameters such as the CP. There are several reasons for studying HOCS: (*i*) it is essential to understanding the behavior of nonlinearly transformed communication signals which are CS [2], (*ii*) it can be used to construct algorithms for signal detection, time-delay estimation, modulation recognition [8, 9], and system identification [3, 5] and, (*iii*) it can be useful in analytical performance evaluations of estimators that operate on CS signals. HOCS is being studied by the authors within the nonstochastic time-average framework, as well as by Giannakis and his group, who use the stochastic process framework.

It is shown that each of the two methods for CP estimation has advantages over the other that depend on the extent of the domain over which the parameter estimate is needed. However, the frequency-domain method can have a serious leakage problem that cannot be fixed, whereas the time-domain method can be modified to substantially reduce leakage at the cost

*This work was jointly supported by the National Science Foundation under grant MIP–91–12800 and the Army Research Office under contract DAAL03–91–C–0018.

of increased computation. Also, in the case of measuring the CP over a large portion of its domain, the frequency-domain method is much more computationally costly than the time-domain method.

The parameters of HOCS are defined in Section 2. Estimators of the CP, their approximate computational costs, and the leakage problem are discussed in Section 3. In Section 4 numerical examples are provided to illustrate the properties of the estimators, and a discussion of the relative merits of the estimators for various situations is contained in Section 5.

## 2 Higher-Order Cyclostationarity

Let $x(t)$ denote a time-series defined for all $t$ such that the parameters in this section exist[1]. The $n$th-order lag product is defined by

$$L_x(t,\tau)_n \triangleq \prod_{j=1}^{n} x(t+\tau_j) \qquad \tau \triangleq [\tau_1 \cdots \tau_n], \tag{1}$$

and its Fourier coefficient is called the cyclic temporal moment function (CTMF),

$$\begin{aligned} R_x^\alpha(\tau)_n &\triangleq \lim_{T\to\infty} \frac{1}{T} \int_{T/2}^{T/2} L_x(t,\tau)_n \, e^{-i2\pi\alpha t}\, dt \\ &\equiv \left\langle L_x(t,\tau)_n e^{-i2\pi\alpha t} \right\rangle_0, \end{aligned} \tag{2}$$

because it is also the Fourier coefficient of the temporal moment function defined by

$$R_x(t,\tau)_n \triangleq \langle L_x(t,\tau)_n \rangle = \sum_\alpha R_x^\alpha(\tau)_n e^{i2\pi\alpha t}, \tag{3}$$

where the sum is over all *cycle frequencies* $\alpha$ for which the CTMF is not identically zero, and $\langle\cdot\rangle$ denotes the multiple-sine-wave (polyperiodic) component extraction operation, which can be interpreted as a temporal expectation operation [2, 4]. The cyclic temporal cumulant function (CTCF),

$$C_x^\beta(\tau)_n \triangleq \left\langle C_x(t,\tau)_n \, e^{-i2\pi\beta t} \right\rangle_0. \tag{4}$$

is the Fourier coefficient of the temporal cumulant function

$$C_x(t,\tau)_n = \sum_{P=\{\nu_k\}_{k=1}^p} \left[ k(p) \prod_{j=1}^{p} R_x(t,\tau_{\nu_j})_{|\nu_j|} \right], \tag{5}$$

where $P$ is the set of distinct partitions $\{\{\nu_j\}_{j=1}^p\}$ of the index set $\{1,2,\cdots,n\}$, $k(p) \triangleq (-1)^{p-1}(p-1)!$, $\tau_{\nu_j}$ is the vector of lags with indices in the partition-element set $\nu_j$, and $|\nu_j|$ is the number of elements in $\nu_j$ [6, 8]. The CTCF can therefore be expressed in terms of lower-order CTMFs:

$$C_x^\beta(\tau)_n = \sum_{P=\{\nu_k\}_{k=1}^p} \left[ k(p) \sum_{\alpha^\dagger \mathbf{1}=\beta} \prod_{j=1}^{p} R_x^{\alpha_j}(\tau_{\nu_j})_{|\nu_j|} \right], \tag{6}$$

where $\mathbf{1} \triangleq [1\cdots 1]$ and $\alpha \triangleq [\alpha_1 \cdots \alpha_p]$. The reduced-dimension (RD) CTCF $\bar{C}_x^\beta(u)_n$ is simply the CTCF with $\tau_i = u_i$ for $i = 1,2,\cdots,n-1$ and $\tau_n = 0$.

In the frequency domain, $n$th-order moments and cumulants are defined in terms of $n$ narrowband time-series with center frequencies $[f_1 \cdots f_n] = \boldsymbol{f}$:

$$X_T(t,f_j) = \int_{t-T/2}^{t+T/2} x(v) e^{-i2\pi f_j v}\, dv. \tag{7}$$

The spectral moment is defined by

$$S_x(\boldsymbol{f})_n \triangleq \lim_{T\to\infty} \left\langle \prod_{j=1}^{n} X_T(t,f_j) \right\rangle_0, \tag{8}$$

and the spectral cumulant is given by the usual combination of lower-order moments (cf. (5)):

$$P_x(\boldsymbol{f})_n = \sum_{P=\{\nu_k\}_{k=1}^p} \left[ k(p) \prod_{j=1}^{n} S_x(\boldsymbol{f}_{\nu_j})_{|\nu_j|} \right]. \tag{9}$$

The spectral moment and cumulant can be represented in the following ways:

$$S_x(\boldsymbol{f})_n = \sum_\alpha \bar{S}_x^\alpha(\boldsymbol{f}')_n \delta(\boldsymbol{f}^\dagger \mathbf{1} - \alpha), \tag{10}$$

$$P_x(\boldsymbol{f})_n = \sum_\beta \bar{P}_x^\beta(\boldsymbol{f}')_n \delta(\boldsymbol{f}^\dagger \mathbf{1} - \beta), \tag{11}$$

where the weighting functions in the spectral cumulant are the cyclic polyspectra given by

$$\begin{aligned} \bar{P}_x^\beta(\boldsymbol{f}')_n &= \int_{-\infty}^{\infty} \bar{C}_x^\beta(u)_n \, e^{-i2\pi u^\dagger \boldsymbol{f}'}\, du \qquad (12) \\ &= \mathcal{F}^{n-1}\{\bar{C}_x^\beta(u)_n\} \qquad (13) \end{aligned}$$

where $\boldsymbol{f}' = [f_1 \cdots f_{n-1}]$, and similarly for the spectral moment function

$$\begin{aligned} \bar{S}_x^\alpha(\boldsymbol{f}')_n &= \int_{-\infty}^{\infty} \bar{R}_x^\alpha(u)_n \, e^{-i2\pi u^\dagger \boldsymbol{f}'}\, du \qquad (14) \\ &= \mathcal{F}^{n-1}\{\bar{R}_x^\alpha(u)_n\}. \qquad (15) \end{aligned}$$

[1] For example, analog amplitude modulated or digital phase-shift-keyed signals [8].

## 3 Cyclic Polyspectrum Estimators

For a given segment of $x(v)$ with length $T$ and center $t$, the estimator for the CTMF is given by

$$R^{\alpha}_{x_T}(t,\tau)_n = \frac{1}{T}\int_{t_l}^{t_u}\prod_{j=1}^{n} x(v+\tau_j)\, e^{-i2\pi\alpha v}\, dv, \quad (16)$$

where $t_l = t - T/2 - \min\{\tau_j\}$, $t_u = t + T/2 - \max\{\tau_j\}$, and $t_u \geq t_l$. If $t_u < t_l$ the estimate is defined to be zero. The estimator for the CTCF is given by the combination of lower-order CTMF estimates

$$C^{\beta}_{x_T}(t,\tau)_n = \sum_{P=\{\nu_k\}_{k=1}^{p}} (-1)^{p-1}(p-1)! \times \left[\sum_{\alpha^{\dagger}\mathbf{1}=\beta}\left(\prod_{j=1}^{p} R^{\alpha_j}_{x_T}(t,\tau_{\nu_j})_{|\nu_j|}\right)\right], \quad (17)$$

as in (6). The CTMF estimator (16) converges pointwise in $t$ to the CTMF (2) and, therefore, the CTCF estimator (17) converges pointwise to the CTCF (4) [7, 8].

As explained in [7, 8], the CP can be estimated by Fourier transforming a windowed estimate of the RD-CTCF:

$$\bar{P}^{\beta}_{x_T}(t,f')_{\Delta f} = \int_{-\infty}^{\infty} w_{1/\Delta f}(u)\bar{C}^{\beta}_{x_T}(t,u)_n e^{-i2\pi u^{\dagger}f'}\, du \quad (18)$$

$$w_{1/\Delta f}(u) = \prod_{j=1}^{n-1}\mathrm{rect}(u_j\Delta f),$$

where $\mathrm{rect}(\cdot)$ is a rectangle that is centered at the origin with unity height and width.

The CP can also be estimated by first constructing the *nth-order cyclic periodogram*

$$I^{\beta}_{x_T}(t,f')_n \triangleq \frac{1}{T}X_T(t,\beta-\mathbf{1}^{\dagger}f')\prod_{j=1}^{n-1}X_T(t,f_j),$$

masking it by a special function $Z_{\beta}(f')$, and then convolving with a multidimensional smoothing window:

$$\bar{P}^{\beta}_{x_T}(t,f')_{\Delta f} = W^{\beta}_{\Delta f}(f') \otimes \left[I^{\beta}_{x_T}(t,f')_n Z_{\beta}(f')\right], \quad (19)$$

where $Z^{\beta}(f')$ is zero for all augmented frequency vectors

$$[f_1 \cdots f_{n-1}\ (\beta - \mathbf{1}^{\dagger}f')]$$

that lie on a *$\beta$-submanifold.* The vector $[g_1 \cdots g_n]$ lies on a $\beta$-submanifold if there is at least one partition $\{\nu_j\}_{j=1}^{p}$ in $P$ with $p > 1$ such that each sum $\alpha_k = \sum_{k\in\nu_j} g_k$ is a $|\nu_j|$th-order cycle frequency of $x(t)$. These $\beta$-submanifolds must be avoided in the convolution because the smoothed $n$th-order cyclic periodogram converges to the function $\bar{S}^{\beta}_{x}(f')_n$, which can contain multiple impulsive factors for values of $f'$ that lie on $\beta$-submanifolds, but which, for all other $f'$, is equal to the nonimpulsive function $\bar{P}^{\beta}_{x}(f')_n$. These impulses are avoided in the method (18) because the additive sine-wave components in the $u$ variables of the RD-CTMF estimate $\bar{R}^{\beta}_{x_T}(t,u)_n$ are removed in forming the RD-CTCF estimate $\bar{C}^{\beta}_{x_T}(t,u)_n$, and it is these additive sine waves that give rise to the (smoothed) spectral lines in the transform $I^{\beta}_{x_T}(t,f')_n$ of $\bar{R}^{\beta}_{x_T}(t,u)_n$.

Submanifolds

The definition of the $\beta$-submanifolds can be understood by reexpressing the RD-CTMF in terms of the RD-CTCF and lower-order CTMFs,

$$R^{\beta}_{x}(\tau)_n = C^{\beta}_{x}(\tau)_n - \sum_{\substack{P\\ p\neq 1}}\left[k(p)\sum_{\alpha^{\dagger}\mathbf{1}=\beta}\prod_{j=1}^{p} R^{\alpha_j}_{x}(\tau_{\nu_j})_{|\nu_j|}\right], \quad (20)$$

where $\tau = [u_1 \cdots u_{n-1}\ 0]$, and Fourier transforming to obtain $\bar{S}^{\beta}_{x}(f')_n$:

$$\bar{S}^{\beta}_{x}(f')_n = \bar{P}^{\beta}_{x}(f')_n - \sum_{\substack{P\\ p\neq 1}}k(p)\sum_{\alpha^{\dagger}\mathbf{1}=\beta} \bar{S}^{\alpha_p}_{x}(f'_{\nu_p})_{|\nu_p|}\prod_{j=1}^{p-1}\left\{\bar{S}^{\alpha_j}_{x}(f'_{\nu_j})_{|\nu_j|}\delta(f^{\dagger}_{\nu_j}\mathbf{1}-\alpha_j)\right\}, \quad (21)$$

where it is assumed that the partition elements are ordered such that $\nu_p$ always contains $\tau_n$ $(= 0)$ in (20), and where

$$\int_{-\infty}^{\infty} R^{\alpha}_{x}(\tau)_n e^{-i2\pi f^{\dagger}\tau}\, d\tau = \bar{S}^{\alpha}_{x}(f')_n\delta(\mathbf{1}^{\dagger}f-\alpha)$$

is used to transform each of the CTMFs in the products in the sum over $P$ in (20), except for the one with reduced dimension, for which (15) is used.

It is clear that $\bar{S}^{\beta}_{x}(f')_n$ equals $\bar{P}^{\beta}_{x}(f')_n$ only if the transform of the sum over $P$ is zero, which will happen if one or more of the impulse functions in (21) is zero. The $\beta$-submanifolds are simply the $f'$ vectors for which there is at least one partition for which there is at least one $\alpha$ such that the argument of each associated impulse function is zero, in which case that impulse is nonzero. It is important to note that the function $\bar{S}^{\beta}_{x}(f')_n$ is *not* impulsive at a value of $f'$ that lies on a $\beta$-submanifold unless all the lower-order coefficients $\bar{S}^{\alpha_j}_{x}(f'_{\nu_j})_{|\nu_j|}$ of the impulses are nonzero.

Thus, by using (19), the CP is estimated without actually estimating a cumulant, but instead by avoiding

the parts of the spectral moment estimate that correspond to the products of lower-order spectral moment estimates that are subtracted in (21).

**Leakage From Submanifolds**

A leakage effect exists in the method (19) that is due to the smearing of the impulses from the $\beta$-submanifolds to neighboring regions off the $\beta$-submanifolds. To see this, the temporal mean of (19) is computed. From [8],

$$I^{\beta}_{x_T}(t, \boldsymbol{f}')_n = \mathcal{F}^{n-1}\{\bar{R}^{\beta}_{x_T}(t, u)_n\},$$

$$\left\langle \bar{R}^{\beta}_{x_T}(t, u)_n \right\rangle_0 = \bar{R}^{\beta}_{x}(u)_n v(u),$$

where

$$v(u) \triangleq \begin{cases} 1 + u_0(u)/T, & |u_0(u)| \le T \\ 0, & \text{otherwise,} \end{cases}$$

and

$$u_0(u) \triangleq \min\{0, u_1, \cdots, u_{n-1}\} - \max\{0, u_1, \cdots, u_{n-1}\}.$$

Using this result, it is easy to show that the temporal mean of (19) is given by the convolution

$$W_{\Delta f}(\boldsymbol{f}') \otimes \left[ (\bar{S}^{\beta}_{x}(\boldsymbol{f}')_n \otimes V(\boldsymbol{f}'))\, Z_{\beta}(\boldsymbol{f}') \right],$$

where $V(\boldsymbol{f}')$ is the $n$-1 dimensional Fourier transform of $v(u)$. The effect of the convolution with $V(\boldsymbol{f}')$ is to smear the impulses in $\bar{S}^{\beta}_{x}(\boldsymbol{f}')_n$, thus producing spectral leakage into nearby regions, which is not removed by the masking function $Z_{\beta}(\boldsymbol{f}')$.

The method (18) also exhibits leakage when the CTMFs (2) are computed using an FFT algorithm, and the cycle frequencies are not "on bin center." This leakage can be substantially reduced by computing each CTMF by evaluating the FST (the Fourier series transform, which is like the DFT, but is a function of a continuous frequency variable), but this will increase the computational cost of the method, as noted in the next section.

**Computational Costs**

The computational requirements of of the CP estimators (18) and (19) are derived in [8] and presented here. The operations count for (18) is derived by assuming that an FFT algorithm is used to compute the transforms in (18) and (2), and the count for (19) is derived by assuming that the FFT is used to compute the transforms (7).

To compute the CP for all values of the discrete normalized-frequency vector $\boldsymbol{f}'$ on the hypercube $[-0.5, 0.5]^{n-1}$, the estimator (18) requires approximately

$$(N_t/N_f)^{n-1}\left[n - 1 + (nA_n/2 + 1)N_t \log N_t\right] + (N_t/N_f)^{n-1} \log(N_t/N_f)^{n-1} + (N_t/N_f)^{n-1} \quad (22)$$

operations, and the estimator (19) requires approximately

$$\left[(n-1) + N_f^{n-1} + nA_n/2\right] N_t^{n-1} + N_t \log N_t \quad (23)$$

operations, where $A_n$ denotes the total number of $\alpha$ such that $\alpha^{\dagger}\mathbf{1} = \beta$. For both methods, $T = N_t T_s$. For the method (18), the width of the tapering window in samples is $N_t/N_f$, which yields a spectral resolution of $\Delta f \approx N_f/(N_t T_s)$, and for the method (19), $T = N_t T_s$, and the width of the spectral smoothing window in samples is $N_f$, which yields a spectral resolution of $\Delta f = N_f/(N_t T_s)$.

The computational cost of the frequency-domain estimator (19) is reduced if only a portion of the CP is needed. For example, if a single frequency in the vector $\boldsymbol{f}'$ is held constant, the computations (23) are reduced by a factor of approximately $N_t$. The cost (22) can also be reduced in this case by computing the FST instead of using a multidimensional FFT to transform the RD-CTCF estimate, but the size of this reduction depends on $N_t$.

Both methods become costlier as the frequency resolution is increased, but at different rates. For example, Figure 1 shows the logarithm of the ratio of the cost (23) to the cost (22) for $n = 4$, $N_t = 1024$, $A_n = 0, 6$, and various $N_f$. Figure 2 shows the same quantity for the case of $N_f = 64$, $n = 4$, $A_n = 0, 6$, and various $N_t$. Observe that the method (19) is always more costly than the method (18).

## 4 Numerical Examples

In this section the errors in several fourth-order CP measurements of the type (19) are displayed graphically for the purpose of illustrating the leakage phenomenon discussed in Section 3.

The signal of interest is a binary pulse-amplitude-modulated signal with symbol-interval length $T_0 = 7$ ($T_s = 1$ here), rectangular pulses rect$(t/T_0)$, and independent identically distributed symbols. It is shown in [8] that the $n$th-order CTCF for this signal exists and is well-behaved, and has cycle frequencies equal to all harmonics of the symbol rate $k/T_0$, but for the purposes of the simulations, only the second-order cycle frequencies for $|k| \le 3$ were used to compute the lower-order CTMFs and to find the $\beta$-submanifolds because the higher harmonics produce relatively weak cyclic features and can, therefore, be neglected. This signal has no cycle frequencies for $n$ odd.

A 1024-point segment of the signal was simulated and the fourth-order CP for $\beta = 0$ and $\beta = 1/T_0$ were computed using the frequency-smoothing (FS)

method (19), (18) with FFTs, and (18) using the FST for estimating the lower-order CTMFs (16). For the time-domain methods, the RD-CTCF was estimated on the cubic grid of integers $\boldsymbol{u} = [u_1\ u_2\ u_3] \in [-8, 7]^3$, and then transformed. In the FS method, the spectral smoothing window width was set equal to 64 samples. Thus, each method uses approximately the same $N_t$ and $N_f$ parameters, and can therefore be compared fairly.

Because computing the entire CP using (19) is prohibitively costly, only two "slices" of the CP were estimated. The slices correspond to $\boldsymbol{f}' = [f_1\ f_2\ 0]$ and $\boldsymbol{f}' = [f_1\ f_2\ 1/T_0]$. The same slices were extracted from the time-domain CP estimates as well, yielding four sets with three slices each. The ideal CP was computed by evaluating the formula given in [8], and then the error in the magnitude of each slice was computed by subtracting measured from ideal. The total error in each slice is determined by averaging the absolute error over all points in the slice, and is shown in Table 1 for the four sets of slices. The table indicates that the time-domain method that uses the FST can outperform the FS method by almost an order of magnitude. The peak error for each slice is shown in Table 2. Each of the peak errors is at or adjacent to the origin.

| $f_3$ | $\beta = 0$ | | | $\beta = 1/T_0$ | | |
|---|---|---|---|---|---|---|
| | FFT | FST | FS | FFT | FST | FS |
| 0 | 1.5 | 1.1 | 4.6 | 3.0 | 0.8 | 5.1 |
| $1/T_0$ | 0.7 | 0.2 | 1.5 | 1.1 | 0.3 | 2.0 |

Table 1: Averaged absolute errors of the CP estimates.

| $f_3$ | $\beta = 0$ | | | $\beta = 1/T_0$ | | |
|---|---|---|---|---|---|---|
| | FFT | FST | FS | FFT | FST | FS |
| 0 | 101 | 101 | 363 | 42 | 7.5 | 122 |
| $1/T_0$ | 5.9 | 2.6 | 38 | 16 | 4.2 | 72 |

Table 2: Peak absolute errors of the CP estimates.

The submanifolds and estimate-error slices for the FS method for $\beta = 0$ are shown in Figures 3 and 4, and for $\beta = 1/T_0$ in Figures 5 and 6. (The submanifolds are depicted in these figures by solid lines.) The strongest leakage occurs around submanifolds that correspond to strong second-order features, that is, to submanifolds with relatively large $\bar{S}_x^{\alpha_j}(f'_{\nu_j})_2$ values. It can be seen from these graphs that the errors are concentrated around the submanifold lines corresponding to $\alpha_j = 0$ and $\alpha_j = 1/T_0$, especially around the intersection of submanifold lines at the origin.

## 5 Discussion

Although the FS method (19) of estimating the CP has serious drawbacks relative to the time-domain method (18), there are some situations in which it could be useful. For example, if it is desired to compute a low-dimensional slice of the CP that is not near submanifolds with a small spectral resolution width, the FS method can require fewer computations.

If the signal of interest has no lower-order CS, then the number of submanifold points is greatly reduced relative to the example in this paper, and therefore the computations involved in determining the submanifolds can be greatly reduced (cf. Figures 1 and 2). However, if there are CS signals with unknown cycle frequencies corrupting the signal of interest, then there will be other sets of submanifolds that will not only increase the amount of leakage, but will give rise to very large estimates at the submanifold points, which are unknown *a priori*. This same problem occurs if the signal of interest is modeled as stationary, but is actually CS. This can be the case, for example, if a phase-randomizing variable is introduced into a stochastic model of the signal in order to render it stationary over the ensemble, because each sample path will still be CS. If the conventional polyspectrum is estimated from a sample path of such a noncycloergodic process, the estimator will produce very large results on the submanifolds, and leakage will be severe.

The time-domain method (18) also suffers when CS signals with unknown parameters corrupt the signal of interest. To circumvent this problem, an algorithm initially developed to perform signal detection in completely unknown environments can be used to estimate all cycle frequencies associated with the data for all orders $n$ less than some integer $N$. The estimated cycle frequencies can then be used in the estimation procedure to produce correct CP estimates [9].

## 6 Conclusions

Difficulties arising from measuring the cyclic polyspectrum using a frequency-smoothed higher-order cyclic periodogram are delineated and illustrated. The first is a large computational cost, and the second is an incurable leakage problem. These two difficulties render the method less attractive than the alternative method of Fourier transforming the tapered cyclic cumulant estimate. The leakage problem is less severe when the signal has no lower-order cyclostationarity,

but is still present for cycle frequency equal to zero, that is, it is present in the conventional polyspectrum for stationary signals. Also, the computational cost of the frequency-smoothing method is relatively high even in the absence of lower-order cyclostationarity.

## References


[1] D.R. Brillinger. "An Introduction to Polyspectra," *Annals of Mathematical Statistics,* Vol. 36, pp. 1351–1374, 1965.

[2] W.A. Gardner. *Statistical Spectral Analysis: A Nonprobabilistic Theory.* Englewood Cliffs, New Jersey: Prentice-Hall 1987.

[3] W.A. Gardner and T.L. Archer. "Exploitation of Cyclostationarity for Identifying the Volterra Kernels of Nonlinear Systems," *IEEE Transactions on Information Theory,* Vol. 39, March 1993 (in press).

[4] W. A. Gardner and W. A. Brown. "Fraction-of-Time Probability for Time-Series that Exhibit Cyclostationarity," *Signal Processing,* Vol. 23, No. 3, pp. 273–292, June 1991 [EURASIP].

[5] G.B. Giannakis and A.V. Dandawate. "Polyspectral Analysis of (Almost) Cyclostationary Signals: LPTV System Identification and Related Applications," in *Proceedings of the Twenty-Fifth Asilomar Conference on Signals, Systems and Computers* Nov. 4-6, 1991, Pacific Grove, CA, pp. 377–382.

[6] A.N. Shiryaev. "Some Problems in the Spectral Theory of Higher-Order Moments — I," *Theory of Probability and Its Applications,* Vol. 5, No. 3, pp. 265–284, 1960.

[7] C.M. Spooner and W.A. Gardner. "Estimation of Cyclic Polyspectra," *Proceedings of the Twenty-Fifth Annual Asilomar Conference on Signals, Systems and Computers,* Nov. 4-6, 1991, Pacific Grove, CA, pp. 370–376.

[8] C.M. Spooner. "Theory and Application of Higher-Order Cyclostationarity," Ph.D. Dissertation, Dept. of Electrical and Computer Engineering, University of California, Davis, CA, June 1992.

[9] C.M. Spooner and W.A. Gardner. "Exploitation of Higher-Order Cyclostationarity for Weak-Signal Detection and Time-Delay Estimation," in *Proceedings of the Sixth Workshop on Statistical Signal & Array Processing,* Oct. 7–9, 1992, Victoria, B.C. Canada, pp. 197–201.

[10] C.M. Spooner and W.A. Gardner. "An Overview of the Theory of Higher-Order Cyclostationarity," in *Proceedings of the NASA/Hampton Workshop on Nonstationary Random Processes,* A. G. Miamee, Editor, Hampton University, Hampton, VA, August 1–2, 1991, pp. 110–125.


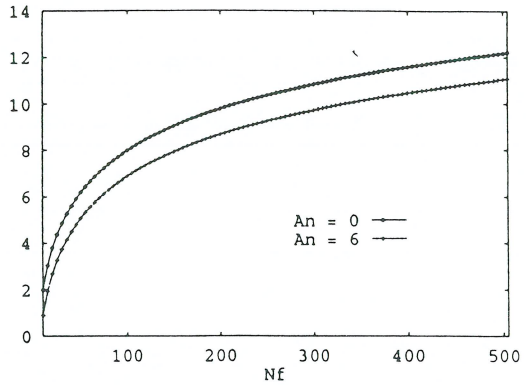


Figure 1: Computational cost (23) for (19) divided by (22) for (18) (log scale) for variable $N_f$.

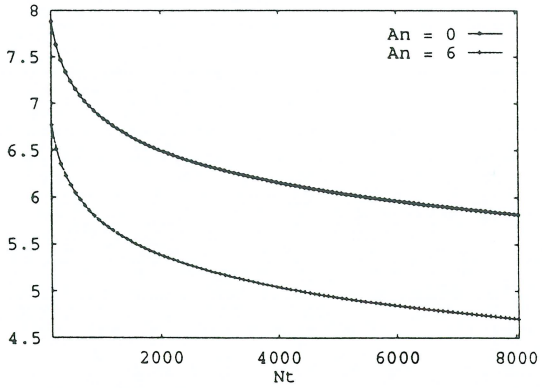


Figure 2: Computational cost (23) for (19) divided by (22) for (18) (log scale) for variable $N_t$.

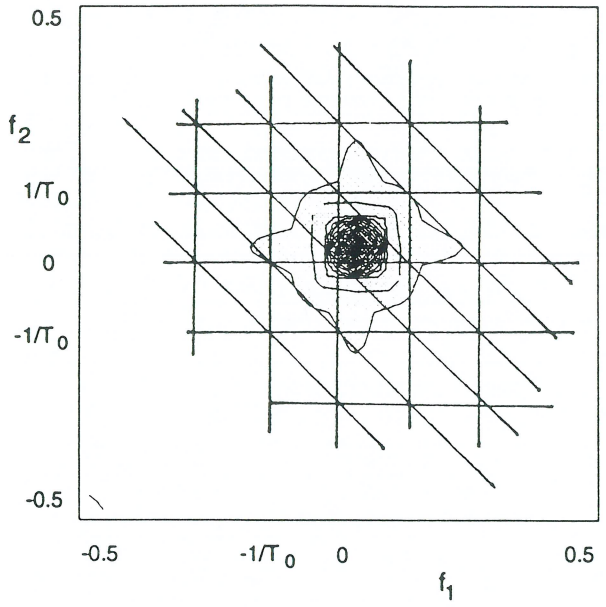


Figure 3: Error contours for the FS method for $\beta = 0$, $f_3 = 0$.

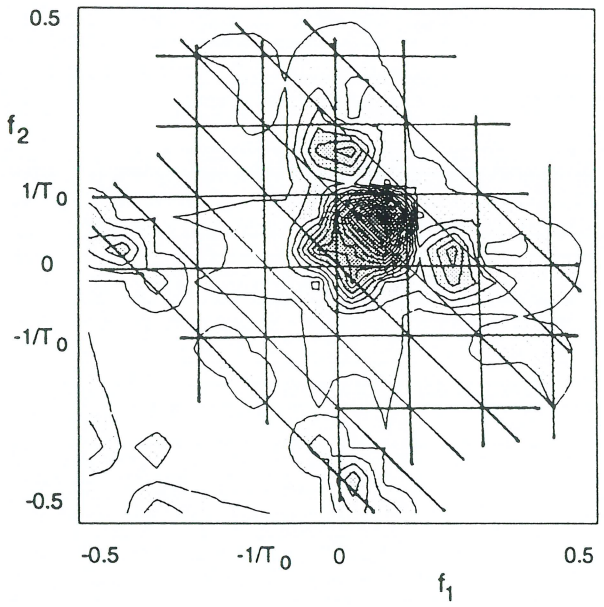


Figure 5: Error contours for the FS method for $\beta = 1/T_0$, $f_3 = 0$.

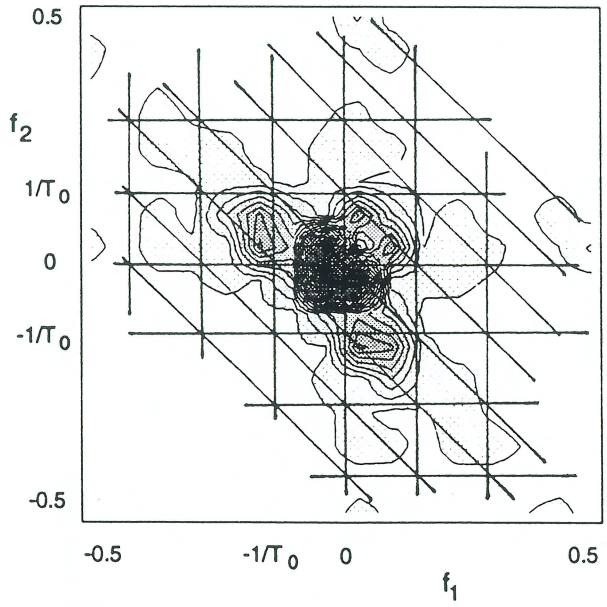


Figure 4: Error contours for the FS method for $\beta = 0$, $f_3 = 1/T_0$.

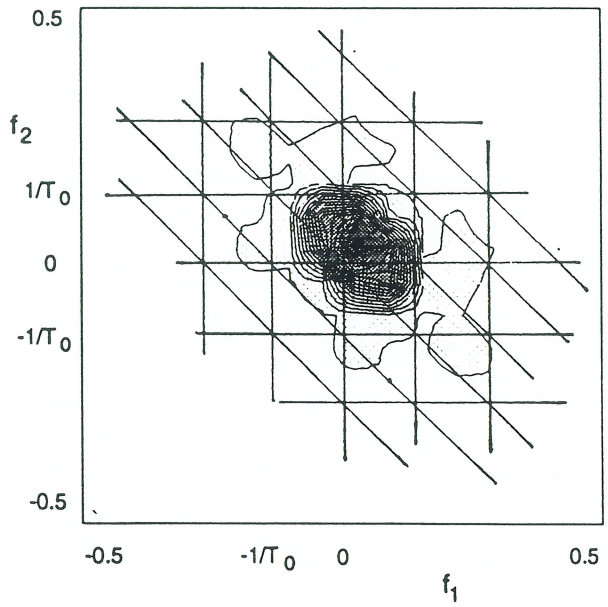


Figure 6: Error contours for the FS method for $\beta = 1/T_0$, $f_3 = 1/T_0$.